Cell Reports

Resource

A Comprehensive Functional Characterization of *Escherichia coli* Lipid Genes

Graphical Abstract

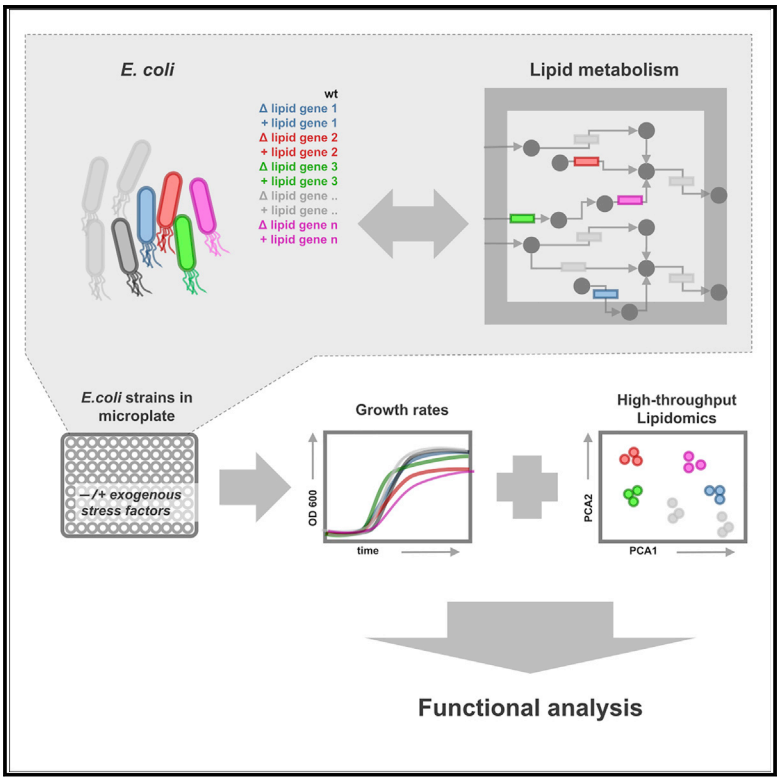

Highlights

- Knockout or overexpression of lipid-related genes leads to distinctive lipidomes
- Links between lipid classes and cell growth are established
- Lipidomic changes due to exogenous stress can be modeled
- High-throughput lipidomics allows the analysis of >300 samples per day

Authors

Aike Jeucken, Martijn R. Molenaar, Chris H.A. van de Lest, Jeroen W.A. Jansen, J. Bernd Helms, Jos F. Brouwers

Correspondence

j.brouwers@uu.nl

In Brief

Jeucken et al. analyzed lipidomes of *E. coli* strains with knockout or overexpression of known lipid-related genes. They demonstrate relationships between lipid species and classes and investigate their link to cell growth. The high-throughput lipidomic method is then used to model lipidomic changes to exogenous alcohols.

Jeucken et al., 2019, Cell Reports *27*, 1597–1606
April 30, 2019
https://doi.org/10.1016/j.celrep.2019.04.018

CellPress

Cell Reports
Resource

A Comprehensive Functional Characterization of *Escherichia coli* Lipid Genes

Aike Jeucken,[1] Martijn R. Molenaar,[1] Chris H.A. van de Lest,[1] Jeroen W.A. Jansen,[1] J. Bernd Helms,[1] and Jos F. Brouwers[1,2,*]

[1]Department of Biochemistry and Cell Biology, Faculty of Veterinary Medicine, Utrecht University, Yalelaan 2, 3584CM Utrecht, the Netherlands

[2]Lead Contact

*Correspondence: j.brouwers@uu.nl

https://doi.org/10.1016/j.celrep.2019.04.018

SUMMARY

Lipid membranes are the border between living cells and their environments. The membrane's lipid composition defines fluidity, thickness, and protein activity and is controlled by the intricate actions of lipid gene-encoded enzymes. However, a comprehensive analysis of each protein's contribution to the lipidome is lacking. Here, we present such a comprehensive and functional overview of lipid genes in *Escherichia coli* by individual overexpression or deletion of these genes. We developed a high-throughput lipidomic platform, combining growth analysis, one-step lipid extraction, rapid LC-MS, and bioinformatic analysis into one streamlined procedure. This allowed the processing of more than 300 samples per day and revealed interesting functions of known enzymes and distinct effects of individual proteins on the phospholipidome. Our data demonstrate the plasticity of the phospholipidome and unexpected relations between lipid classes and cell growth. Modeling of lipidomic responses to short-chain alcohols provides a rationale for targeted membrane engineering.

INTRODUCTION

Escherichia coli (*E. coli*) is a popular biological production platform, but particularly the recombinant production of eukaryotic membrane proteins and achieving high titers of hydrophobic compounds remain challenging because of their interaction with membrane phospholipids (Atsumi et al., 2008; Baumgarten et al., 2017; Choi and Lee, 2013; Rau et al., 2016; Schlegel et al., 2014; Yang et al., 2018). Many membrane proteins require a specific lipid context for optimal function (Wikström et al., 2009). The selective barrier function of membranes can be compromised by the production of non-physiological (levels of) hydrophobic compounds (Sikkema et al., 1995). For instance, the formation of respiratory chain supercomplexes depends on the presence of cardiolipin (CL) (Mileykovskaya and Dowhan, 2014; Pfeiffer et al., 2003). Likewise, many membrane proteins bind lipids selectively to modulate their structure and function (Laganowsky et al., 2014). Therefore, a thorough understanding of the phospholipidome is a prerequisite for the optimal exploitation of the potential of *E. coli* as a biotechnological platform.

Understanding how the phospholipidome is controlled has been hampered mainly by two difficulties: (1) the complexity of the phospholipidome and (2) the large number of enzymes involved in lipid metabolism. The complexity of the phospholipidome results from the presence of a variety of headgroups that are combined with one to four fatty acyl chains of various chain lengths, degrees of unsaturation, and presence of cyclopropane groups (Hartler et al., 2017; Matyash et al., 2008; Murphy and Axelsen, 2011). Consequently, the lipidome of *E. coli* may consist of several thousand lipid species, making the lipidome more complex than the (water-soluble) metabolome (Dowhan, 2017; Sud et al., 2007; Weaver et al., 2014). The major lipid classes in *E. coli* are phosphatidylethanolamine (PE), phosphatidylglycerol (PG), and CL (Dowhan, 2013). Minor lipid classes such as *N*-acylated PE (acyl-PE) and *O*-acylated PG (acyl-PG) have also been identified, but ^{32}P studies have shown that many more minor classes are yet to be identified (Cho et al., 1973; Garrett, 2016; Mileykovskaya et al., 2009) (Raetz, 1986). To date, 70 proteins have been shown to be involved in the synthesis, modification, and degradation of lipids in *E. coli*, each lipid being a substrate for multiple enzymes and enzymes acting on multiple lipid species (Kanehisa, 2002). The public availability of comprehensive collections of knockout strains and plasmids for overproduction has allowed the successful high-throughput screening of *E. coli* genes to elucidate the roles of enzymes (Baba et al., 2006; Babu et al., 2018; Baran et al., 2013; Fuhrer et al., 2017; Kim et al., 2017; Kitagawa et al., 2005; Sévin et al., 2017). However, a detailed analysis of the influence of lipid catabolic and anabolic proteins on the phospholipidome is missing because of the lack of suitable high-throughput methods for lipid extraction, analysis, and data interpretation (Hyötyläinen et al., 2017; Lísa and Holčapek, 2015; Schwudke et al., 2017; Simons, 2018).

Here, we present a high-throughput method for lipid analysis that has allowed us to analyze the phospholipidome of wild-type (WT) *E. coli* as well as all known lipid gene-overexpressing mutants and all viable lipid gene knockouts. This approach revealed previously unknown functions for lipid catabolic and anabolic enzymes (here referred to as lipid enzymes). Unexpected relations were found between lipid classes and cell growth. Most important, our approach unveiled an essential lipid-modifying enzyme framework that can be manipulated for

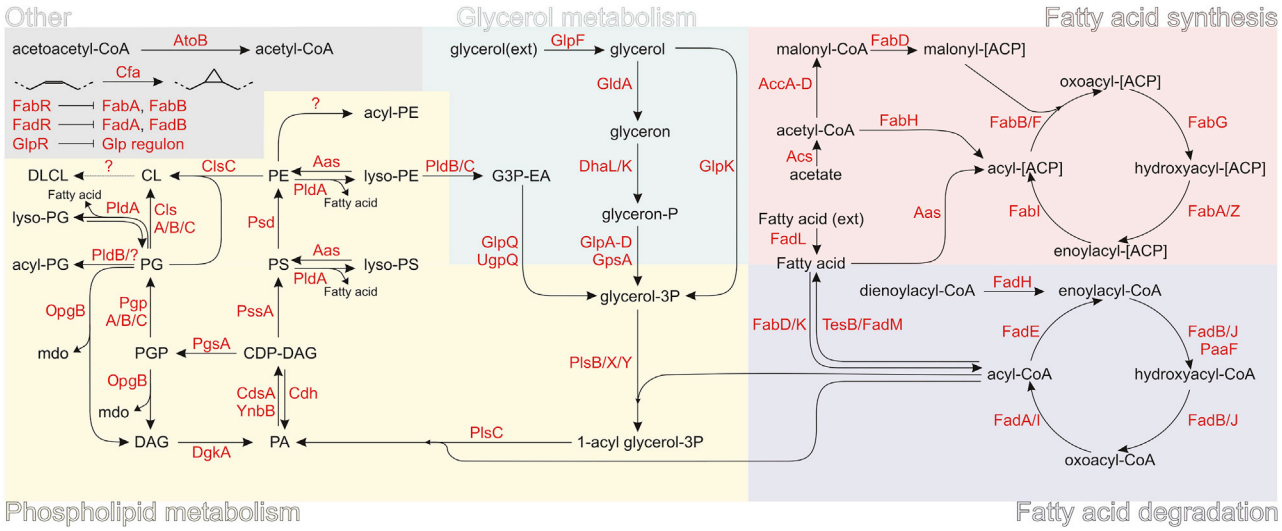

Figure 1. Lipid Pathways in *E. coli*

Reactions are classified in five categories, displayed in different background colors. These colors are consistently used in the other figures for enzymes belonging to the corresponding category.

rational targeted membrane engineering and better exploitation of *E. coli* as a production platform.

RESULTS

A High-Throughput Method for Lipidomic Analysis of *E. coli* Mutants

By combining lipid-enzyme activities reported in the Kyoto Encyclopedia of Genes and Genomes (KEGG) pathways (Kanehisa and Goto, 2000) with current literature, we constructed a schematic overview of lipid metabolism in *E. coli* in which the lipid enzymes were classified in five pathway groups (Figure 1; Table S1). In order to study the effect of these *E. coli* lipid enzymes on the lipidome and bacterial growth rates, we developed a high-throughput lipidomic platform (see Figure 2A for a schematic overview). We grew triplicates of the 67 lipid enzyme overexpression transformants and the corresponding 46 viable single-gene knockout mutants in multi-well plates in a thermostatic plate reader. Measuring the optical density at 600 nm (OD_{600}) at 5 min intervals, we recorded detailed growth rates of all strains until the stationary phase was reached (Figure S1). Transferring the cultures to glass-coated plates allowed subsequent, in-plate, one-step lipid extraction (see Figure S2 for a comparison with the established Bligh and Dyer and methyl tert-butyl ether [MTBE] lipid extraction methods; Bligh and Dyer, 1959; Matyash et al., 2008). In our one-step protocol, the protein-free chloroform and methanol mixture was injected directly onto the liquid chromatography-mass spectrometry (LC-MS) column. In a run time of only 4 min, we achieved a headgroup-based separation of lipids (Brouwers et al., 2013). By matching with our *in silico*-generated lipid database, 226 molecular species from ten lipid classes were identified (Figure 2B; see Figure S3 for MS2 confirmation). Because growth was also measured, this allows linking growth to detailed lipidomic data. The full dataset and lipid database are available (Data S3, S4, and S5).

A Rich Variety of Distinct Lipidomes

Principal-component analysis (PCA) of lipidomes of each of the lipid enzyme-overexpressing strains demonstrated a direct link between enzyme levels and the resulting phospholipidome. Overexpression of individual lipid enzymes led to a very reproducible shift in lipidome, shown as a distribution over the full area of the PCA score plot (Figure 3A). The corresponding (Pareto-scaled) PCA loading plot (Figure 3B) shows a scattering of lipid species. This demonstrates that the abundance of each lipid species in the lipidome is controlled differently by the concerted action of lipid enzymes. We calculated the Euclidean distance between each overexpressing strain and WT *E. coli* from the first three principal components, which accounted for 62% of the total variance in the dataset (Figure 3C). The top five of the thus identified lipidomes that were most different from WT *E. coli* belonged to four different pathways: phospholipid metabolism (Aas, YnbB), fatty acid synthesis (Aas, FabH), glycerol metabolism (GlpD), and fatty acid degradation (FadJ). The most distant lipidome results from overexpression of Aas (bifunctional protein Aas, acyl-ACP synthase). Aas is a reported acyltransferase that acylates the acyl carrier protein involved in fatty acid elongation. However, Aas is best known for its acylation of lysophospholipids to their diacyl analogs (Jackowski et al., 1994). Unexpectedly, the levels of diacyl PE and PG were much lower in this strain (-16.3% [$p < 0.01$] and -11.7% [$p < 0.001$], respectively), and the abundance of the third largest phospholipid, CL, was only fractionally higher (Figures S4A–S4C). Overexpression of Aas resulted in the abundant presence of two headgroup acylated lipid classes (acyl-PG and acyl-PE, both approximately 15%) (Figures S4D and S4E). Remarkably, both lipid classes were hardly detectable in WT *E. coli* and most other strains.

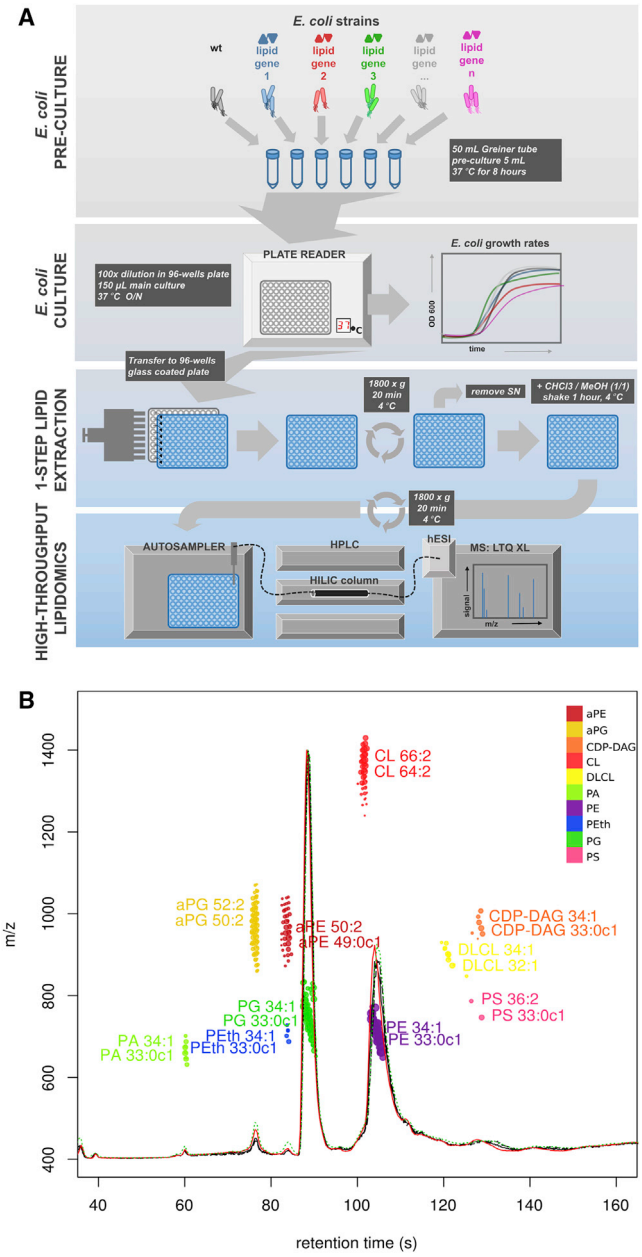

Figure 2. High-Throughput Lipidomic Platform to Analyze *E. coli* Lipid Species and Growth

(A) Schematic overview of the applied method that allows high-throughput growth and lipid analysis.

(B) Lipid classes and species identified in this study. The base peak chromatogram of all overexpressing strains is plotted as an overlay. The two most abundant molecular species of each lipid class are labeled. Lipid classes are indicated with different colors, and these colors are consistently used in the other figures.

Hence, Aas proves to be a promiscuous and potent acyltransferase. Apart from the changes related to its intrinsic acyltransferase activity, Aas overexpression also affected phospholipid unsaturation and cyclopropane formation but not average acyl chain length (Figures S4F–S4H). Similar to Aas, the other four enzymes at highest Euclidean distance to WT *E. coli* (i.e., GlpD, FadJ, FabH, and YnbB) displayed changes to WT *E. coli* lipidome that were prominent in both lipid class distribution and acyl composition (Figure S4).

As with lipid enzyme overexpression, knockout of single-lipid genes gave rise to a wide variety of distinct but reproducible lipidomes, which further confirmed that the *E. coli* lipidome is the result of a complex interaction of many lipid enzymes (Figures 3D and 3E). Deletion of either *fabH* or *cfa* resulted in particularly distinct lipidomes, as confirmed by the high Euclidean distance of these lipidomes to the WT *E. coli* lipidome (Figure 3F). Notably, two of the five knockouts resulting into the most distinct lipidomes were related to the first steps in fatty acid synthesis (*fabH* and *fabF*). However, their effects on lipid class distribution and acyl properties were markedly different (Figure S5). For instance, whereas *fabH* knockout resulted in longer acyl length than in WT *E. coli*, acyl chains were shorter in *fabF* knockouts. This may be related to the much higher CL content of the latter compared with the *fabH* knockout, as we observed a consistent link between the abundance of CL and short acyl chains (discussed below). Knockout of *pldB*, currently annotated as a lysophospholipase, suggested a different role for this enzyme, as it accumulated large quantities of acyl-PG but not acyl-PE (Figures S5D and S5E). This suggests that acyl-PG is predominantly degraded by the phospholipase PldB. The lack of acyl-PE accumulation suggests that another enzyme is responsible for the hydrolysis of this amide bond, possibly by a yet to be identified fatty acid amide hydrolase homolog. Of the knockout strains, the *cfa* knockout had the most distinct lipidome compared with WT and showed a reduced presence of cyclopropane rings and a concomitant increased unsaturations in acyl chains. At the lipid class level, *cfa* knockout showed an increased CL abundance at the expense of PG but not PE. This suggests that the enzyme primarily responsible for CL synthesis from PG, ClsA, has a preference for straight chain-containing rather than cyclopropane-containing fatty acyls.

The Lipid Pathway-Lipidome Interplay

Enzyme levels of each of the five lipid pathways of Figure 1 affected the composition of every lipid class (Figure 4A). Dissection of the chord diagram and zooming in on the phospholipases PldA and PldB clearly showed the differences in substrates for these two enzymes with similar activity (Figure 4B). Deletion of *pldA* resulted in an increased level of multiple CL species and thus suggested CL to be a substrate of PldA. This is in agreement with the observation that total CL levels increase upon *pldA* deletion and decrease upon overexpression (Data S1C). On the other hand, *pldB* deletion was strongly correlated to an increased amount of multiple acyl-PG species (discussed above) but also to a decreased level of di-Lyso-CL (DLCL) species (Figure 4B). This suggests that PldB is also involved in the deacylation of CL to DLCL.

Lipid Molecular Species

A correlation heatmap of the 100 most abundant lipid species shows a strong and consistent correlation between PE and PG species with corresponding acyl composition (Figure 5). This is

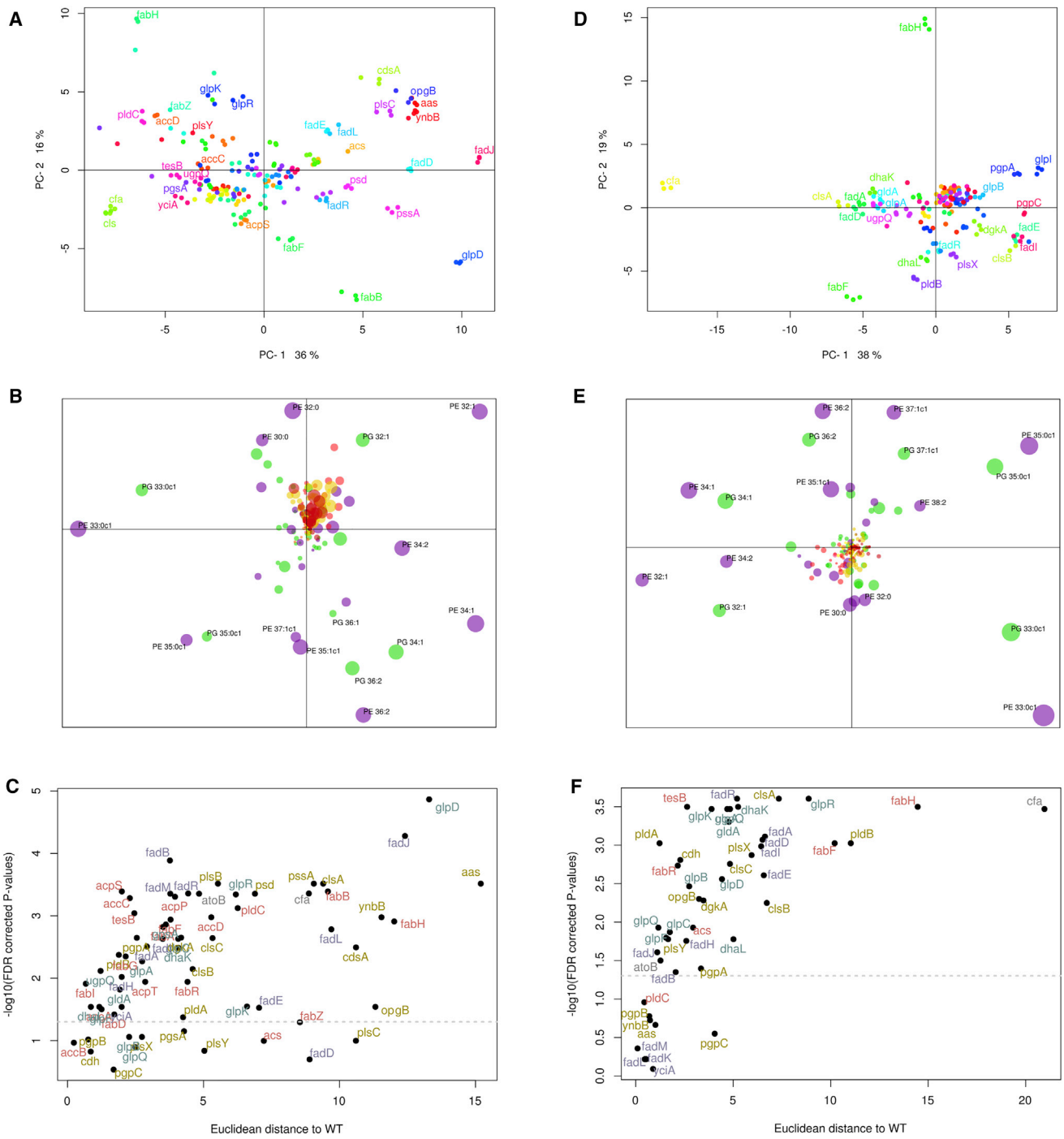

Figure 3. Lipidome Changes in *E. coli* with Altered Lipid Enzyme Expression

(A) Principal-component analysis (PCA) score plot of single lipid enzyme-overexpressing strains.

(B) PCA loading plot of overexpressing strains; the sizes of the dots correspond to relative abundance, and lipid species that contributed most to the variance are labeled.

(C) Dissimilarity (distance) and corresponding statistical significance of lipid enzyme-overexpressing strains and WT *E. coli* containing the empty vector used for overexpression.

(D) PCA score plot of *E. coli* lipidomes with indicated single-gene deletions.

(E) PCA loading plot resulting from single gene deletions.

(F) Dissimilarity (distance) and corresponding statistical significance of single-gene deletions and WT *E. coli*.

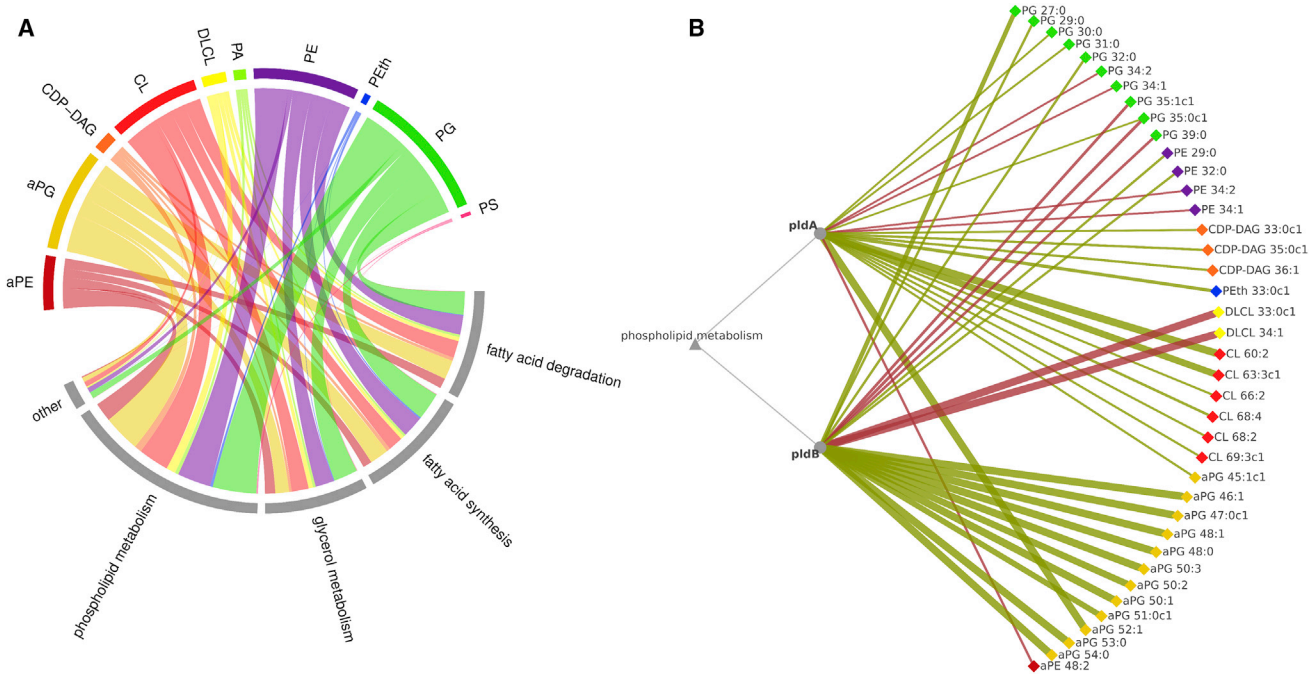

Figure 4. Interactions between Lipids and Pathways

(A) Chord diagram connecting lipid species that changed ($p < 0.05$) upon either overexpression or deletion of a single-lipid gene and the corresponding pathway.
(B) Top 20 most significantly altered lipid species after knockout of pldA or pldB.

in line with the PCA loading plots, in which these PE and PG species mapped close together (Figures 3B and 3E). Although this may at first seem self-evident because both lipid classes are synthesized from the same pool of cytidine diphosphate diacylglycerol (CDP-DAG), it should be noted that in eukaryotes, the Lands cycle results in extensive remodeling of lipid species and lipid class-specific fingerprints (Chen et al., 2007; Lands, 1958; Wang et al., 2012; Wu et al., 2016). Thus, the combined activity of PldA and Aas is not a substitute for the Lands cycle in this bacterium. Notably, a class-specific acyl composition was observed for CL, which contained short acyl chains with few cyclopropane moieties (Figure S6). Hence, there appears to be a species specificity in CL synthases (ClsA being the most active), opposite to the enzymes involved in PE and PG synthesis.

Mathematical Modeling of the *E. coli* Lipidome

We then wondered whether we could reliably model the lipidome of *E. coli* in response to exogenous stress factors. This can be particularly useful in engineering *E. coli* membrane composition when used as a production platform for hydrophobic compounds. For instance, short-chain alcohols have great economic value and can be produced by the organism. These alcohols can serve directly as bio-fuels in conventional combustion engines or may be used as resource for synthesis of more complex biomolecules (Green, 2011; Harvey and Meylemans, 2011; Procentese et al., 2017; Shen and Liao, 2008). To test the effect of these alcohols on the *E. coli* lipidome, we exposed growing bacteria to concentrations leading to approximately 30% growth inhibition: methanol (C1, 4.5% v/v), ethanol (C2, 3.0% v/v), n-propanol (C3, 1.0% v/v), and n-butanol (C4, 0.3% v/v). We then analyzed the corresponding lipidomes. Because cyclopropane fatty acids have been suggested to increase alcohol tolerance in prokaryotes (Kanno et al., 2013), we also included the Cfa-overexpressing strain.

PCA of the thus obtained lipidomes identified two major lipidome-discriminating factors (Figures 6A and 6B). The first, corresponding to principal component 1, separates empty vectors from Cfa overexpression. The Cfa-overexpressing strains are located at the left of the score plot (Figure 6A), and as expected, this corresponded to higher abundance of cyclopropane-containing lipid species at the left site of the corresponding loading plot (Figure 6B). In principal component 2, we observed a relationship between the chain length of the supplied alcohol, with shorter alcohol chain lengths corresponding to higher principal component 2 values and, arguably, longer fatty acyl lengths in the lipid species (Figures 6A and 6B, respectively). To further investigate this relationship, we constructed a mixed linear model to calculate expected lipid species abundance from its lipid class, chain length, unsaturation, cyclopropane presence, alcohol chain length, Cfa overexpression, and the interactions among these factors. The final model was obtained by minimizing the Akaike information criterion (Akaike, 1998). This model with data transformations, correlations, and intercepts is shown in Data S2. The correlation coefficient (r) between experimental data and modeled data was 0.82, and the residuals had a close to normal distribution (represented by the straight line in Figure 6C). Within this model, a very strong correlation was found

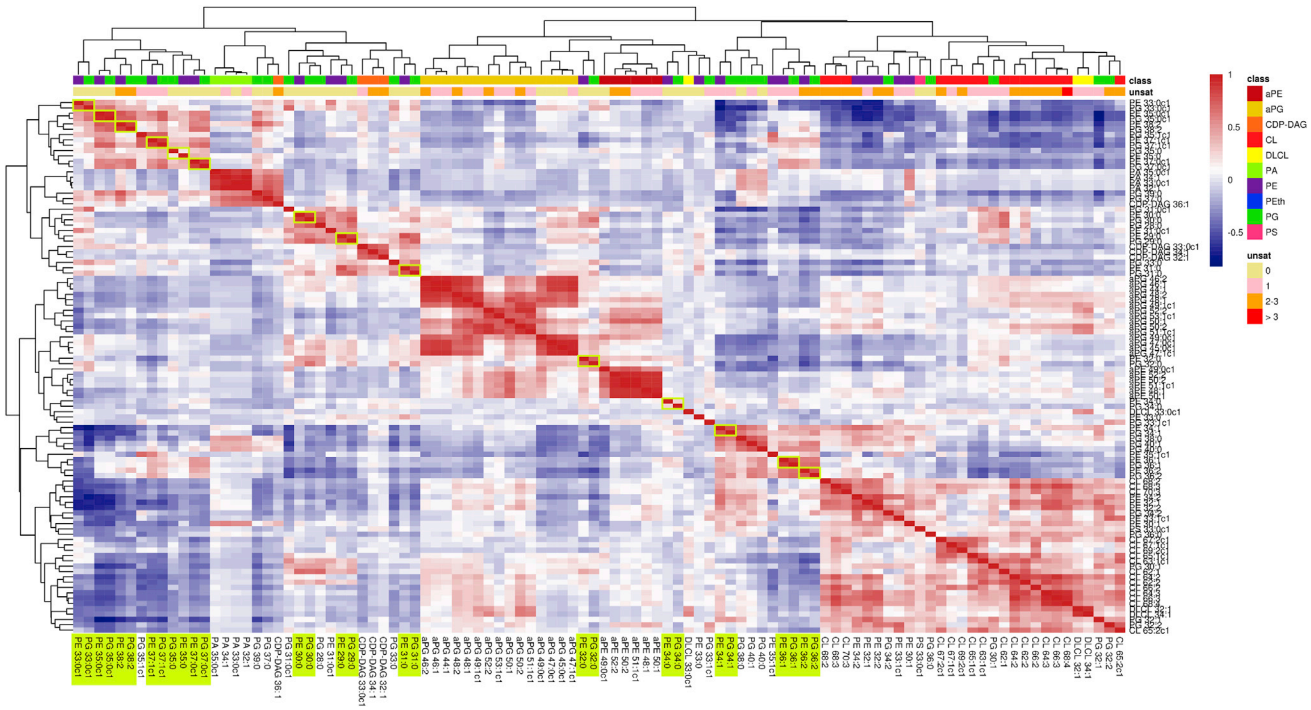

Figure 5. Heatmap of Lipid-Lipid Correlations of the 100 Most Abundant Lipid Species

Lipid ordering is based on hierarchical clustering. Highlighted are the close correlations of PE and PG species with identical acyl composition. Correlations were calculated on the basis of all lipidomic analysis of genetic constructs (n > 300).

between the alcohol chain length and the interaction of this parameter with the phospholipid carbon number ($r = -0.987$; Data S2). The nature of this interaction can be visualized (Figure 6D). This confirmed the observations from the PCA: particularly in the extremes of the fatty acyl carbon numbers, increasing alcohol chain length results in a shift toward shorter phospholipid acyl chains.

The Relation between Bacterial Growth Rate and Lipidome Composition

Many overexpressing strains had altered growth rates compared with WT *E. coli*, but we did not observe a clear correlation between changed growth rates and lipid pathways (Figure 7A). ClsB, one of the three known CL synthases, was the only enzyme whose overexpression resulted in a more than 5% growth rate increase ($p < 0.05$). Interestingly, the ClsB-overexpressing strain uniquely had the capacity to synthesize phosphatidylethanol (PEth) (Data S1G). This lipid class is presumably synthesized by a combination of CL synthase-associated PLD activity and the presence of ethanol from the stock solution of the antibiotic used in the growth medium. Absence of PEth in any other strain demonstrates that this is a unique activity of ClsB and that ClsB is expressed at low levels in all other strains, including WT *E. coli* (Jeucken et al., 2018). None of the single-gene knockout strains showed an increased growth rate (Figure 7B), and remarkably, only 9% of the knockouts had a growth inhibition of more than 20%, demonstrating the high capacity of *E. coli* to handle lipidomic changes. Correlating lipid classes and acyl properties to bacterial growth, we found that phosphatidic acid (PA) and acyl-PE abundance in the lipidome correlated positively with growth rate (Figures 7C and 7D). The positive effect of PA may be linked to the negative correlation existing between CDP-DAG and growth rate, because PA and CDP-DAG are each other's direct precursor and product in a delicate equilibrium (Dowhan, 2013; Kong et al., 2017). In future construction of production strains of *E. coli* it may therefore be of interest to monitor and adapt the levels of these two lipids, by tweaking the expression levels of proteins we here identified to affect these lipids.

DISCUSSION

With this single study we have substantially expanded the current knowledge on *E. coli* lipid metabolism by profiling the lipidome of 113 strains. This became feasible because we developed a high-throughput lipidomic strategy in combination with a tailored lipid database. Previously unresolved minor lipid classes reported in the literature could now be identified, such as CDP-DAG, DLCL, acyl-PG and acyl-PE (Raetz, 1986).

The need for comprehensive lipid profiling in *E. coli* and the richness of the resulting dataset is illustrated by the fact that we discovered several strong clues for previously undescribed enzyme activities and substrate specificities (Aas, ClsB, PldA, PldB). These enzyme activities can be exploited in different fields of biotechnological applications. The potent acyl transferase Aas, but also the lipases PldA and PldB, can prove to be valuable assets in the biotechnological production process of acylated

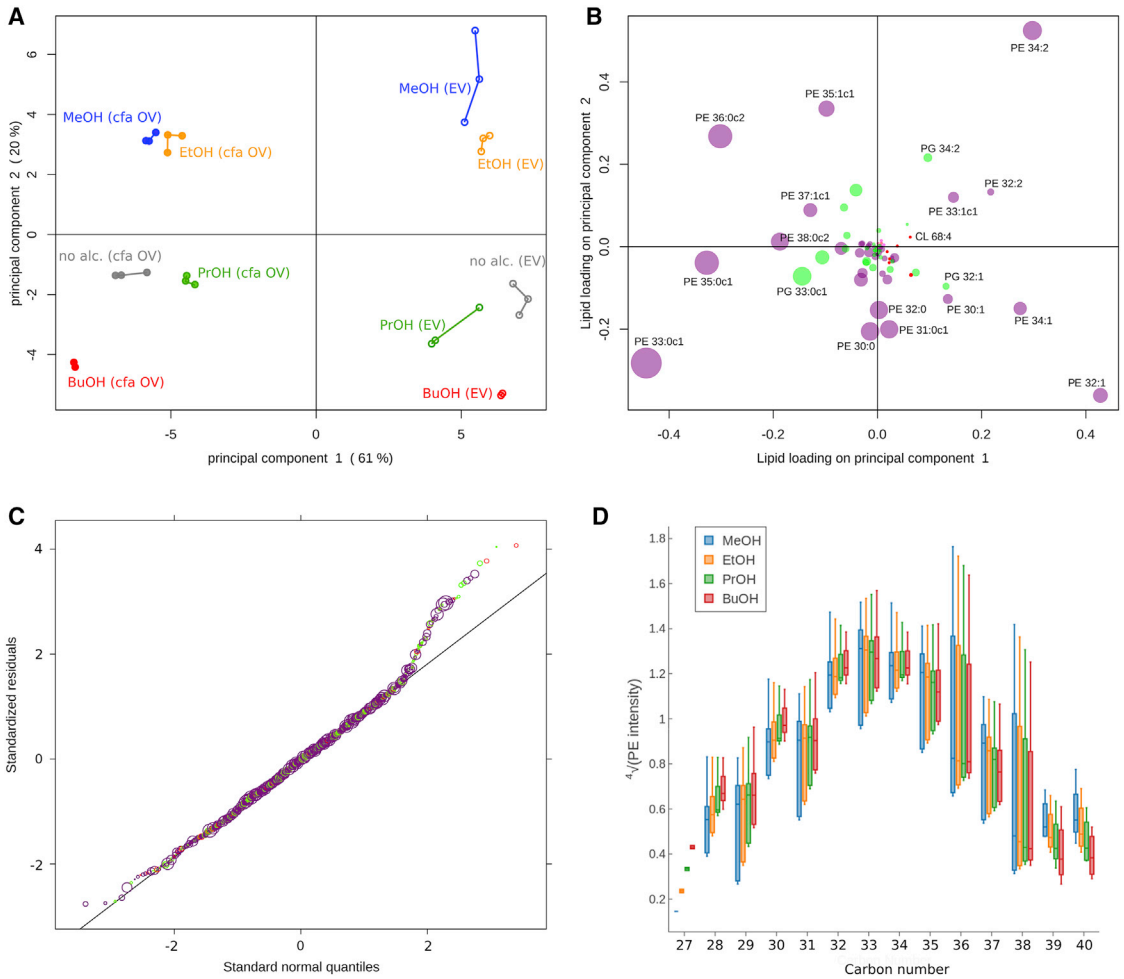

Figure 6. Lipidomic Changes upon Exposure to Linear Short-Chain Alcohols

(A) PCA score plot demonstrating a dependence of principal component 1 on the overexpression of Cfa. Values of principal component 2 proved to be dependent on carbon length of the alcohol.

(B) Lipid loadings on principal components. In general, cyclopropane-containing lipid species had negative loadings on principal component 1, leading to lower principal component 1 values for Cfa-overexpressing samples. Note that phospholipid chain length appears to decrease with increasing alcohol chain length (decreasing principal component 2).

(C) Quantile-quantile plot of residuals of 1,502 modeled lipid species. Lipid color coding is as in (B).

(D) Predicted intensities of PE species of different acyl chain length upon exposure to alcohols. Particularly at the extreme carbon numbers (27–28 and 39–40), it is visible how PE acyl chains shift toward shorter length with increasing alcohol chain length. Error bars represent the 95% confidence interval.

pharmaceuticals (Gotor-Fernández et al., 2006; Patel, 2018). The exciting field of minimal, synthetic organisms can benefit from our findings on ClsB (Stano and Luisi, 2013). As a single enzyme, ClsB allows the synthesis of a variety of phospholipid classes controlled by the availability of primary alcohols. Interestingly, many drastic changes in the lipidome composition hardly affected growth under our experimental conditions. The ample plasticity of the *E. coli* lipidome and the organisms capacity to effectively deal with different environments are exemplified by the ratios between the highest and lowest relative abundance of lipid classes in Data S1. These ratios go from relatively low for PE and PG content, 1.5 and 2, respectively, to more than 50 for the other lipid classes. Also the fatty acid properties length, number of unsaturated carbon-carbon bonds, and number of cyclopropane groups were found to be very flexible (Data S1). It remains to be established whether *E. coli* has a similar tolerance toward lipidomic changes when growing under harsher, physiological conditions. We have demonstrated that the lipidome of *E. coli* can be reliably modeled if a good training dataset is provided.

The triad of lipid gene, lipidome, and growth rate is an important step in moving lipidomics from a descriptive to a functional technique. The detailed lipidomic analysis allows the calculation of derived parameters such as membrane thickness (acyl chain length) and fluidity (degree of unsaturation, cyclopropane occurrence, and lipid class). Together, this enables the rational design of specifically engineered membranes for optimally fitting the goal of the use of a bacterial strain, for instance, the production

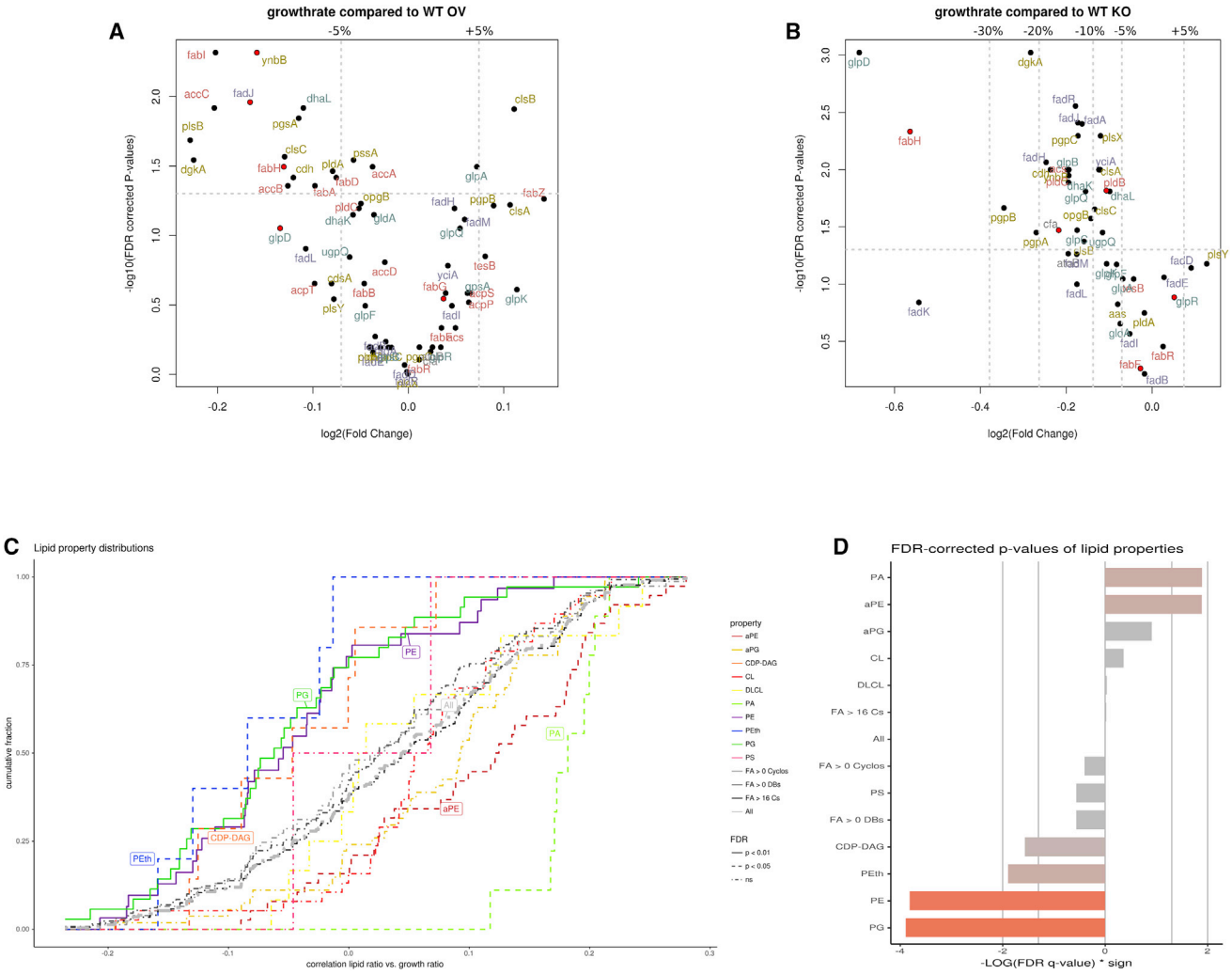

Figure 7. Effects of Lipid-Associated Genetic Perturbations on *E. coli* Growth Rate

(A) Volcano plot of changes in growth rates upon overexpression of individual lipid enzymes. Red dots correspond to strains with most dissimilar lipidomes (cf. Figure 3C). Vertical lines correspond to a decrease or increase in growth rate of 5%.

(B) Volcano plot of changes in growth rates of single lipid-gene knockouts. Vertical lines correspond to the indicated changes in growth rate.

(C and D) Cumulative distributions of Pearson correlation coefficients between individual lipid ratios and *E. coli* growth ratios and corresponding statistics. (C) Distributions are shown for ten different lipid classes and three pre-defined fatty acyl chain properties (colored) or for all studied lipids (gray). (D) Bar plot with log-transformed false discovery rate (FDR)-corrected p values multiplied by the growth-rate direction of the analyzed lipid-associated properties; colors are scaled proportional from gray to red. Horizontal lines indicate p value cutoffs of 0.01 and 0.05 for both directions.

of membrane-destabilizing hydrophobic compounds or foreign membrane proteins (Choi et al., 2017). Moreover, lipidomic data can now be added to a genome-scale model (GEM) (Feist et al., 2007; Price et al., 2004), which has already many times proved to successfully predict strains with increased target (non-physiological) metabolites (Feist and Palsson, 2008).

The high-throughput lipidomic platform is easily applicable to other biological systems, including those with more complex lipidomes (Arroyo-Olarte et al., 2015; Jeucken and Brouwers, 2019). Moreover, the approach described here can directly be combined with other technologies, including large drug screens, RNAi studies, automated microscopic cell screening, and comprehensive inter-omics approaches.

STAR★METHODS

Detailed methods are provided in the online version of this paper and include the following:

- KEY RESOURCES TABLE
- CONTACT FOR REAGENT AND RESOURCE SHARING
- EXPERIMENTAL MODEL DETAILS
  - Plasmids –
  - Growth Conditions –
- METHOD DETAILS
  - Lipid Extraction –
  - Liquid Chromatography Mass Spectrometry of Lipids –

- QUANTIFICATION AND STATISTICAL ANALYSIS
  - Data analysis –

SUPPLEMENTAL INFORMATION

Supplemental Information can be found online at https://doi.org/10.1016/j.celrep.2019.04.018.

ACKNOWLEDGMENTS

We thank Dr. B.M. Gadella and Dr. J.J. van Hellemond for critically reading the manuscript. We thank the people from EdgeLeap (Utrecht, the Netherlands) for their help with network visualizations. This research was funded by grant BB/2012-10047 of the Bio-Based Ecologically Balanced Sustainable Industrial Chemistry (BE-BASIC) project to J.B.H. and J.F.B. and by a Fulbright scholarship to AJ.

AUTHOR CONTRIBUTIONS

Conceptualization, J.F.B. and A.J.; Methodology, M.R.M., J.W.A.J., C.H.A.L., A.J., and J.F.B.; Investigation, A.J. and J.W.A.J.; Data Analysis, A.J., M.R.M., C.H.A.L., and J.F.B.; Writing – Original Draft, A.J. and J.F.B.; Writing – Review & Editing, J.B.H. and J.F.B.; Funding Acquisition, J.B.H. and J.F.B.; Supervision, J.B.H. and J.F.B.

DECLARATION OF INTERESTS

The authors declare no competing interests.

Received: October 29, 2018
Revised: February 25, 2019
Accepted: April 2, 2019
Published: April 30, 2019

SUPPORTING CITATIONS

The following reference appears in the Supplemental Information: Bates et al., (2015).

REFERENCES

Akaike, H. (1998). Information theory and an extension of the maximum likelihood principle. In Selected Papers of Hirotugu Akaike, E. Parzen, K. Tanabe, and G. Kitagawa, eds. (Springer), pp. 199–213.

Arroyo-Olarte, R.D., Brouwers, J.F., Kuchipudi, A., Helms, J.B., Biswas, A., Dunay, I.R., Lucius, R., and Gupta, N. (2015). Phosphatidylthreonine and lipid-mediated control of parasite virulence. PLoS Biol. *13*, e1002288.

Atsumi, S., Hanai, T., and Liao, J.C. (2008). Non-fermentative pathways for synthesis of branched-chain higher alcohols as biofuels. Nature *451*, 86–89.

Baba, T., Ara, T., Hasegawa, M., Takai, Y., Okumura, Y., Baba, M., Datsenko, K.A., Tomita, M., Wanner, B.L., and Mori, H. (2006). Construction of Escherichia coli K-12 in-frame, single-gene knockout mutants: the Keio collection. Mol. Syst. Biol. *2*, 2006.0008.

Babu, M., Bundalovic-Torma, C., Calmettes, C., Phanse, S., Zhang, Q., Jiang, Y., Minic, Z., Kim, S., Mehla, J., Gagarinova, A., et al. (2018). Global landscape of cell envelope protein complexes in Escherichia coli. Nat. Biotechnol. *36*, 103–112.

Baran, R., Bowen, B.P., Price, M.N., Arkin, A.P., Deutschbauer, A.M., and Northen, T.R. (2013). Metabolic footprinting of mutant libraries to map metabolite utilization to genotype. ACS Chem. Biol. *8*, 189–199.

Bates, D., Maechler, M., Bolker, B., and Walker, S. (2015). Fitting linear mixed-effects models using lme4. J. Stat. Softw. *67*, 1–48.

Baumgarten, T., Schlegel, S., Wagner, S., Löw, M., Eriksson, J., Bonde, I., Herrgård, M.J., Heipieper, H.J., Nørholm, M.H.H., Slotboom, D.J., and de Gier, J.W. (2017). Isolation and characterization of the *E. coli* membrane protein production strain Mutant56(DE3). Sci. Rep. *7*, 45089.

Bligh, E.G., and Dyer, W.J. (1959). A rapid method of total lipid extraction and purification. Can. J. Biochem. Physiol. *37*, 911–917.

Brouwers, J.F., Aalberts, M., Jansen, J.W.A., van Niel, G., Wauben, M.H., Stout, T.A.E., Helms, J.B., and Stoorvogel, W. (2013). Distinct lipid compositions of two types of human prostasomes. Proteomics *13*, 1660–1666.

Chen, Q., Kazachkov, M., Zheng, Z., and Zou, J. (2007). The yeast acylglycerol acyltransferase LCA1 is a key component of Lands cycle for phosphatidylcholine turnover. FEBS Lett. *581*, 5511–5516.

Cho, K.S., Benns, G., and Proulx, P. (1973). Formation of acyl phosphatidyl glycerol by Escherichia coli extracts. Biochim. Biophys. Acta. *326*, 355–360.

Choi, Y.J., and Lee, S.Y. (2013). Microbial production of short-chain alkanes. Nature *502*, 571–574.

Choi, K.R., Shin, J.H., Cho, J.S., Yang, D., and Lee, S.Y. (2017). Systems metabolic engineering of Escherichia coli. Ecosal Plus *7*.

Dowhan, W. (2013). A retrospective: use of Escherichia coli as a vehicle to study phospholipid synthesis and function. Biochim. Biophys. Acta *1831*, 471–494.

Dowhan, W. (2017). Understanding phospholipid function: why are there so many lipids? J. Biol. Chem. *292*, 10755–10766.

Feist, A.M., and Palsson, B.Ø. (2008). The growing scope of applications of genome-scale metabolic reconstructions using Escherichia coli. Nat. Biotechnol. *26*, 659–667.

Feist, A.M., Henry, C.S., Reed, J.L., Krummenacker, M., Joyce, A.R., Karp, P.D., Broadbelt, L.J., Hatzimanikatis, V., and Palsson, B.Ø. (2007). A genome-scale metabolic reconstruction for Escherichia coli K-12 MG1655 that accounts for 1260 ORFs and thermodynamic information. Mol. Syst. Biol. *3*, 121.

Fuhrer, T., Zampieri, M., Sévin, D.C., Sauer, U., and Zamboni, N. (2017). Genomewide landscape of gene-metabolome associations in *Escherichia coli*. Mol. Syst. Biol. *13*, 907.

Garrett, T.A. (2016). Major roles for minor bacterial lipids identified by mass spectrometry. Biochim. Biophys. Acta Mol. Cell Biol. Lipids *1862*, 1319–1324.

Gotor-Fernández, V., Brieva, R., and Gotor, V. (2006). Lipases: useful biocatalysts for the preparation of pharmaceuticals. J. Mol. Catal., B Enzym. *40*, 111–120.

Green, E.M. (2011). Fermentative production of butanol–the industrial perspective. Curr. Opin. Biotechnol. *22*, 337–343.

Hartler, J., Triebl, A., Ziegl, A., Trötzmüller, M., Rechberger, G.N., Zeleznik, O.A., Zierler, K.A., Torta, F., Cazenave-Gassiot, A., Wenk, M.R., et al. (2017). Deciphering lipid structures based on platform-independent decision rules. Nat. Methods *14*, 1171–1174.

Harvey, B.G., and Meylemans, H.A. (2011). The role of butanol in the development of sustainable fuel technologies. J. Chem. Technol. Biotechnol. *86*, 2–9.

Hyötyläinen, T., Ahonen, L., Pöhö, P., and Orešič, M. (2017). Lipidomics in biomedical research-practical considerations. Biochim. Biophys. Acta Mol. Cell Biol. Lipids *1862*, 800–803.

Jackowski, S., Jackson, P.D., and Rock, C.O. (1994). Sequence and function of the aas gene in Escherichia coli. J. Biol. Chem. *269*, 2921–2928.

Jeucken, A., and Brouwers, J.F. (2019). High-throughput screening of lipidomic adaptations in cultured cells. Biomolecules *9*, 42.

Jeucken, A., Bernd Helms, J., and Brouwers, J.F. (2018). Cardiolipin synthases of Escherichia coli have phospholipid class specific phospholipase D activity dependent on endogenous and foreign phospholipids. Biochim. Biophys. Acta Mol. Cell Biol. Lipids *1863*, 1345–1353.

Kanehisa, M. (2002). The KEGG database. Novartis Found. Symp. *247*, 91–101, discussion 101–103, 119–128, 244–252.

Kanehisa, M., and Goto, S. (2000). KEGG: Kyoto Encyclopedia of Genes and Genomes. Nucleic Acids Res. *28*, 27–30.

Kanno, M., Katayama, T., Tamaki, H., Mitani, Y., Meng, X.Y., Hori, T., Narihiro, T., Morita, N., Hoshino, T., Yumoto, I., et al. (2013). Isolation of butanol- and

isobutanol-tolerant bacteria and physiological characterization of their butanol tolerance. Appl. Environ. Microbiol. *79*, 6998–7005.

Kim, S., Jeong, H., Kim, E.Y., Kim, J.F., Lee, S.Y., and Yoon, S.H. (2017). Genomic and transcriptomic landscape of Escherichia coli BL21(DE3). Nucleic Acids Res. *45*, 5285–5293.

Kitagawa, M., Ara, T., Arifuzzaman, M., Ioka-Nakamichi, T., Inamoto, E., Toyonaga, H., and Mori, H. (2005). Complete set of ORF clones of Escherichia coli ASKA library (a complete set of E. coli K-12 ORF archive): unique resources for biological research. DNA Res. *12*, 291–299.

Kolde, R. (2015). pheatmap: Pretty Heatmaps. https://CRAN.R-project.org/package=pheatmap.

Kong, P., Ufermann, C.-M., Zimmermann, D.L.M., Yin, Q., Suo, X., Helms, J.B., Brouwers, J.F., and Gupta, N. (2017). Two phylogenetically and compartmentally distinct CDP-diacylglycerol synthases cooperate for lipid biogenesis in *Toxoplasma gondii*. J. Biol. Chem. *292*, 7145–7159.

Laganowsky, A., Reading, E., Allison, T.M., Ulmschneider, M.B., Degiacomi, M.T., Baldwin, A.J., and Robinson, C.V. (2014). Membrane proteins bind lipids selectively to modulate their structure and function. Nature *510*, 172–175.

Lands, W.E. (1958). Metabolism of glycerolipides; a comparison of lecithin and triglyceride synthesis. J. Biol. Chem. *231*, 883–888.

Wilkinson, L. (2011). Venn and Euler data diagrams. https://pdfs.semanticscholar.org/a755/3b15557a82ffc4ea8435f130f3953b48461e.pdf.

Lísa, M., and Holčapek, M. (2015). High-throughput and comprehensive lipidomic analysis using ultrahigh-performance supercritical fluid chromatography-mass spectrometry. Anal. Chem. *87*, 7187–7195.

Matyash, V., Liebisch, G., Kurzchalia, T.V., Shevchenko, A., and Schwudke, D. (2008). Lipid extraction by methyl-tert-butyl ether for high-throughput lipidomics. J. Lipid Res. *49*, 1137–1146.

Mileykovskaya, E., and Dowhan, W. (2014). Cardiolipin-dependent formation of mitochondrial respiratory supercomplexes. Chem. Phys. Lipids *179*, 42–48.

Mileykovskaya, E., Ryan, A.C., Mo, X., Lin, C.C., Khalaf, K.I., Dowhan, W., and Garrett, T.A. (2009). Phosphatidic acid and N-acylphosphatidylethanolamine form membrane domains in Escherichia coli mutant lacking cardiolipin and phosphatidylglycerol. J. Biol. Chem. *284*, 2990–3000.

Murphy, R.C., and Axelsen, P.H. (2011). Mass spectrometric analysis of long-chain lipids. Mass Spectrom. Rev. *30*, 579–599.

Patel, R.N. (2018). Biocatalysis for synthesis of pharmaceuticals. Bioorg. Med. Chem. *26*, 1252–1274.

Pauling, J.K., Hermansson, M., Hartler, J., Christiansen, K., Gallego, S.F., Peng, B., Ahrends, R., and Ejsing, C.S. (2017). Proposal for a common nomenclature for fragment ions in mass spectra of lipids. PLoS ONE *12*, e0188394.

Pfeiffer, K., Gohil, V., Stuart, R.A., Hunte, C., Brandt, U., Greenberg, M.L., and Schägger, H. (2003). Cardiolipin stabilizes respiratory chain supercomplexes. J. Biol. Chem. *278*, 52873–52880.

Price, N.D., Reed, J.L., and Palsson, B.Ø. (2004). Genome-scale models of microbial cells: evaluating the consequences of constraints. Nat. Rev. Microbiol. *2*, 886–897.

Procentese, A., Raganati, F., Olivieri, G., Russo, M.E., de la Feld, M., and Marzocchella, A. (2017). Renewable feedstocks for biobutanol production by fermentation. N. Biotechnol. *39* (*Pt A*), 135–140.

R Development Core Team (2016). R: A language and environment for statistical computing.https://www.r-project.org.

Raetz, C.R.H. (1986). Molecular genetics of membrane phospholipid synthesis. Annu. Rev. Genet. *20*, 253–295.

Rau, M.H., Calero, P., Lennen, R.M., Long, K.S., and Nielsen, A.T. (2016). Genome-wide Escherichia coli stress response and improved tolerance towards industrially relevant chemicals. Microb. Cell Fact. *15*, 176.

Schlegel, S., Hjelm, A., Baumgarten, T., Vikström, D., and de Gier, J.-W. (2014). Bacterial-based membrane protein production. Biochim. Biophys. Acta *1843*, 1739–1749.

Schwudke, D., Shevchenko, A., Hoffmann, N., and Ahrends, R. (2017). Lipidomics informatics for life-science. J. Biotechnol. *261*, 131–136.

Sévin, D.C., Fuhrer, T., Zamboni, N., and Sauer, U. (2017). Nontargeted in vitro metabolomics for high-throughput identification of novel enzymes in Escherichia coli. Nat. Methods *14*, 187–194.

Shannon, P., Markiel, A., Ozier, O., Baliga, N.S., Wang, J.T., Ramage, D., Amin, N., Schwikowski, B., and Ideker, T. (2003). Cytoscape: a software environment for integrated models of biomolecular interaction networks. Genome Res. *13*, 2498–2504.

Shen, C.R., and Liao, J.C. (2008). Metabolic engineering of Escherichia coli for 1-butanol and 1-propanol production via the keto-acid pathways. Metab. Eng. *10*, 312–320.

Sikkema, J., de Bont, J.A., and Poolman, B. (1995). Mechanisms of membrane toxicity of hydrocarbons. Microbiol. Rev. *59*, 201–222.

Simons, K. (2018). How can omic science be improved? Proteomics *18*, e1800039.

Smith, C.A., Want, E.J., O'Maille, G., Abagyan, R., and Siuzdak, G. (2006). XCMS: processing mass spectrometry data for metabolite profiling using nonlinear peak alignment, matching, and identification. Anal. Chem. *78*, 779–787.

Stacklies, W., Redestig, H., Scholz, M., Walther, D., and Selbig, J. (2007). pcaMethods—a bioconductor package providing PCA methods for incomplete data. Bioinformatics *23*, 1164–1167.

Stano, P., and Luisi, P.L. (2013). Semi-synthetic minimal cells: origin and recent developments. Curr. Opin. Biotechnol. *24*, 633–638.

Sud, M., Fahy, E., Cotter, D., Brown, A., Dennis, E.A., Glass, C.K., Merrill, A.H., Jr., Murphy, R.C., Raetz, C.R.H., Russell, D.W., and Subramaniam, S. (2007). LMSD: LIPID MAPS structure database. Nucleic Acids Res. *35*, D527–D532.

Tautenhahn, R., Böttcher, C., and Neumann, S. (2008). Highly sensitive feature detection for high resolution LC/MS. BMC Bioinformatics *9*, 504.

Wang, L., Shen, W., Kazachkov, M., Chen, G., Chen, Q., Carlsson, A.S., Stymne, S., Weselake, R.J., and Zou, J. (2012). Metabolic interactions between the Lands cycle and the Kennedy pathway of glycerolipid synthesis in Arabidopsis developing seeds. Plant Cell *24*, 4652–4669.

Weaver, D.S., Keseler, I.M., Mackie, A., Paulsen, I.T., and Karp, P.D. (2014). A genome-scale metabolic flux model of Escherichia coli K-12 derived from the EcoCyc database. BMC Syst. Biol. *8*, 79.

Wikström, M., Kelly, A.A., Georgiev, A., Eriksson, H.M., Klement, M.R., Bogdanov, M., Dowhan, W., and Wieslander, A. (2009). Lipid-engineered Escherichia coli membranes reveal critical lipid headgroup size for protein function. J. Biol. Chem. *284*, 954–965.

Wu, H., Bogdanov, M., Zhang, Y., Sun, K., Zhao, S., Song, A., Luo, R., Parchim, N.F., Liu, H., Huang, A., et al. (2016). Hypoxia-mediated impaired erythrocyte Lands' cycle is pathogenic for sickle cell disease. Sci. Rep. *6*, 29637.

Yang, J.E., Park, S.J., Kim, W.J., Kim, H.J., Kim, B.J., Lee, H., Shin, J., and Lee, S.Y. (2018). One-step fermentative production of aromatic polyesters from glucose by metabolically engineered Escherichia coli strains. Nat. Commun. *9*, 79.

STAR★METHODS

KEY RESOURCES TABLE

REAGENT or RESOURCE	SOURCE	IDENTIFIER
Bacterial and Virus Strains		
Bacterial strains and plasmids used in this study are listed in Table S2.		N/A
Chemicals, Peptides, and Recombinant Proteins		
Isopropyl -D-1-thiogalactopyranoside (IPTG)	Melford	Art.nr.: I56000-5.0
Chloramphenicol	Roche Diagnostics	Art.nr. 634 433
Kanamycin	Sigma	Art.nr. K1377
Software and Algorithms		
data analysis	R Development Core Team, 2016	R version 3.4.2
XCMS	Smith et al., 2006; Tautenhahn et al., 2008	N/A
venneuler	Kolde, 2015	r package
pheatmaps	Wilkinson, 2011	r package
pcaMethods	Stacklies et al., 2007	r package
cytoscape	Shannon et al., 2003	N/A
Other		
glass coated 96 wells plates conical bottom	Thermofisher	cat# 60180-P304
Kinetex® 2.6 μm HILIC 100, LC Column 50 × 4.6 mm	Phenomenex	Art.nr.: 00B-4461-E0
SecurityGuard ULTRA Cartridges UHPLC HILIC 4.6mm ID Columns, 3/Pk	Phenomenex	Art Nr: AJ0-8772
SecurityGuard ULTRA Holder, for UHPLC Columns 2.1 to 4.6mm ID, Ea	Phenomenex	Art.nr.: AJ0-9000

CONTACT FOR REAGENT AND RESOURCE SHARING

Further information and requests for resources and reagents should be directed to and will be fulfilled by the Lead Contact, Jos F. Brouwers (j.brouwers@uu.nl).

EXPERIMENTAL MODEL DETAILS

Plasmids –

Plasmids for overexpressing the lipid genes were isolated from AG1 (ME5305) host cells, part of the ASKA(-) collection (Kitagawa et al., 2005). These pCA24N plasmids were used to transform BW25113 cells.

The used knockout mutants are part of the Keio collection (Baba et al., 2006), including BW25113 as the adequate control.

Growth Conditions –

Liquid LB medium (10 g/l Trypton, 10 g/l NaCl, 5 g/l yeast extract) was used in all cultures of *E. coli*. For solid medium 15 g/l agar was added. All growth was performed at 37°C. For strain selection purposes medium was supplemented with 34 μg/ml chloramphenicol or 50 μg/ml kanamycin. Final concentration of 10 μM IPTG was used for induction of protein expression for the ASKA(-) clones since the ORFs on the pCA24N plasmid are under control of IPTG-inducible promoter, $P_{T5\text{-}lac}$. 150 μL cultures were grown in 96 wells plates in a Versamax microtiter plate reader (Molecular Devices, Sunnyvale, CA). The plate was covered using a clear film. The growth was closely followed by measuring absorbance at 600 nm every 5 minutes, from which maximum specific growth rates were calculated as the slope of a linear fit to log transformed OD values.

METHOD DETAILS

Lipid Extraction –

Bacterial cultures were transferred to glass coated 96 wells plates with conical bottom, and centrifuged (1800 g, 20min, 4°C). The obtained pellets were resuspended in 150 μl chloroform/methanol (1:1 v/v), extracted for 1h at 4°C, followed by centrifugation (1800 g, 20min, 4°C). The plate was covered by a sheet of aluminum foil and placed in the autosampler.

Liquid Chromatography Mass Spectrometry of Lipids –

Chromatography of 10 μl of the supernatant was performed on a hydrophilic interaction liquid chromatography (HILIC) column (2.6 μm HILIC 100 Å, 50 × 4.6 mm, Phenomenex, Torrance, CA). Lipid classes were separated by gradient elution on a Dionex Ultimate 3000 RS UPLC (ThermoFisher Scientific, Waltham, MA). Solvent A consisted of acetonitrile/acetone (9:1, v/v) whereas solvent B consisted of acetonitrile/H2O (7:3, v/v) with 10mM ammonium formate. Both solvents were with 0.1% formic acid. Flow rate was constant at 1 mL/min, and the gradient was as follows (time in min, %B): (0, 0), (1, 50), (3, 50), (3.1, 100), (4, 100). Subsequent samples were injected without re-equilibration of the column.

The column outlet of the LC was connected to a heated electrospray ionization (HESI) source of a LTQ XL mass spectrometer (ThermoFisher Scientific, Waltham, MA) operated in negative ionization mode. Source- and capillary temperatures were set to 450°C and 400°C, respectively and the ionization voltage to −2.5 kV. Full scan spectra were collected in the range from 350–1750 or 450-1150 amu at a scan speed of 3 scans/s.

High resolution MS2 was used for confirmation of lipid classes. In this case the outlet of the LC was connected to a heated electrospray ionization (HESI) source of an Orbitrap Fusion mass spectrometer. Temperatures for the vaporizer and ion transfer tube were 275°C and 380°C, respectively. Parallelized data dependent MS2 experiments were done with HCD fragmentation set at 30V, using the dual stage linear ion trap to generate up to 30 spectra per second with the resolution parameter set at 'standard'.

In case of the *E. coli* samples grown in the presence of short chain-alcohols the LC outlet was connected to the atmospheric pressure chemical ionization source of the LTQ-XL mass spectrometer.

To quantify lipids, response factors were calculated using authentic lipid standards for CL, PE and PG. The response factor of PG was also used for PA and phosphatidylalcohols. DLCL, CDP-DAG were quantified using the response factor of CL because of lack of available standards.

QUANTIFICATION AND STATISTICAL ANALYSIS

Data analysis –

Data was analyzed using R version 3.4.2 (R Development Core Team, 2016). Data were converted to mz(X)ML format and analyzed using XCMS version 1.52.0 (Smith et al., 2006; Tautenhahn et al., 2008). Resulting raw data are given in Data S3 (growth rates and lipid data) and Data S5 (lipidomic changes induced by alcohols). All statistical analyses were based on triplicate cultures of individual (genetic) conditions. In very few cases, one of the cultures showed no growth and was omitted from further analysis. Standard deviation (SD) was used for error bars throughout the manuscript. Statistical significance was defined as $p < 0.05$, after multiple testing correction for a false discovery rate of 0.05 were applicable. Euler diagrams, heatmaps and principal component analysis were constructed and visualized with the R packages 'venneuler', 'pheatmaps' and 'pcaMethods', respectively (Kolde, 2015; Wilkinson, 2011; Stacklies et al., 2007). The open source application "Cytoscape" was used to construct chord diagrams (Shannon et al., 2003). Despite the existence of comprehensive lipid databases (Pauling et al., 2017; Sud et al., 2007), we constructed a new *in-silico* database because of the absence of several lipid classes (e.g., acyl PG, PEth and DLCL) and cyclopropane moieties from them. Recombination of fatty acids with chain lengths from 12 to 20, zero or one unsaturation and zero or one cyclopropane moieties, glycerol phosphate and known head groups were made, and the resulting masses and structure formulas were calculated (Data S4). The presence of a cylcopropane moiety was assumed for lipid species with uneven carbon numbered acyl chains.